Silver Nanoparticles Coated with Thioxanthone Derivative as Hybrid Photoinitiating Systems for Free Radical Polymerization

ARTICLE *in* LANGMUIR · DECEMBER 2012

Impact Factor: 4.46 · DOI: 10.1021/la303923p · Source: PubMed

5 AUTHORS, INCLUDING:

Raphaël Schneider
University of Lorraine
202 PUBLICATIONS **2,616** CITATIONS
SEE PROFILE

Lavinia Balan
French National Centre for Scientific Research
134 PUBLICATIONS **1,212** CITATIONS
SEE PROFILE

Langmuir

Article

pubs.acs.org/Langmuir

Silver Nanoparticles Coated with Thioxanthone Derivative as Hybrid Photoinitiating Systems for Free Radical Polymerization

Emilie Nehlig,[†] Raphaël Schneider,[†] Loic Vidal,[‡] Gilles Clavier,[§] and Lavinia Balan*[,‡]

[†]Laboratoire Réactions et Génie des Procédés, Université de Lorraine, CNRS UPR 3349, 1 rue Grandville, 54001 Nancy, France

[‡]Institut de Science des Matériaux de Mulhouse, CNRS LRC 7228, 15 rue Jean Starcky, 68057 Mulhouse, France

[§]PPSM, ENS Cachan, CNRS, UniverSud, 61 avenue President Wilson, 94230 Cachan, France

ABSTRACT: A new type of photoinitiator for free radical polymerization was synthesized and characterized. 2-(11-Mercaptoundecyloxy)thioxanthone (**1**) was anchored at the surface of silver nanoparticles (NPs), and the interaction of plasmon field generated in the immediate vicinity of Ag NPs carrying the chromophores was evaluated. The optical features and structure of the silver-initiator nanoassemblies (Ag@**1**) were characterized by UV−vis and fluorescence spectroscopy, X-ray diffraction (XRD), transmission electron microscopy (TEM), and X-ray photoelectron spectroscopy (XPS). TEM and XRD studies revealed the presence of ca. 5−6 nm diameter Ag NPs, and XPS also confirmed the successful anchorage of **1** at their periphery. The nanoassemblies Ag@**1** were successfully used as macroinitiator for radical polymerization of acrylate monomers, triggered photochemically, to obtain Ag(0)−polyacrylate nanocomposite materials. The nanocomposite materials synthesized with the use of Ag@**1** exhibit attractive possibilities for patterning the surface of thin films.

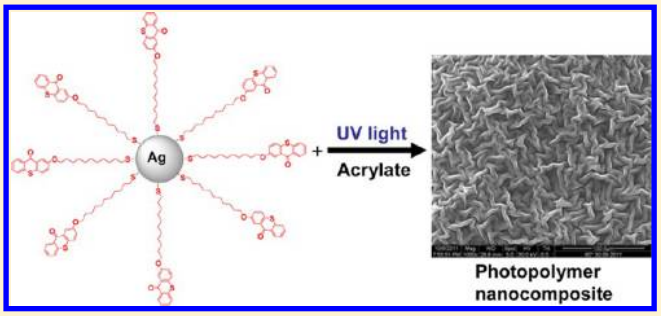

1. INTRODUCTION

Because of their attractive applications in electronics, optics, catalysis, and biotechnology, metal nanoparticles−polymer composites have attracted intense research interest in recent years.[1−3] Successful synthesis of high quality composites largely depends on particle size, content, and dispersity in the polymer matrix, the latter generally being a bottleneck for nanocomposite preparation.

Two different approaches have been developed to achieve silver nanoparticle−polymer composites. During the past 10 years, many efforts have been devoted to the *in situ* synthesis of silver nanoparticles in polymer matrixes, which involves the dissolution and the reduction (chemical reduction, photoreduction, or thermal decomposition) of Ag^+ salts or complexes.[4−11] A second, less common, method involves polymerizing the matrix around nanoparticles by using ligands compatible with the polymerizable formulation.[12−14] Thiol-capped Ag nanoparticles with narrow size distribution are easy to synthesize and fairly stable.[13−16] The surface of Ag nanoparticles can thus be modified by functional groups allowing the controlled change of the properties of the particles and the customization of the surface in view of further reactions.

Like benzophenone, benzyl, and quinones, thioxanthone [TX]C═O and its derivatives are type II photoinitiators and initiate radical polymerization by H-abstraction (Scheme 1). Upon light excitation, the triplet state of [TX]C═O readily reacts with H-donor compounds such as tertiary amines, thiols, ethers, and alcohols to yield the initiating radicals.[17−20]

Scheme 1. Mechanism for the Radical Photopolymerization of a Monomer Initiated by a TX Derivative

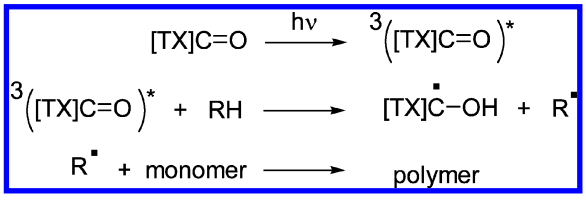

Because many thioxanthone derivatives can operate in the UV region of the spectrum, it is not surprising that these compounds have gained a great interest in many fields such as coating technologies, adhesives, microelectronic components, or photoresists.

In a continuing effort to develop novel photoinitiator structure and metal nanoparticles−polymer composites, we synthesized 2-(11-mercaptoundecyloxy)thioxanthone (**1**) and anchored this compound at the surface of silver nanoparticles (Figure 1). The synthetic procedure involved the replacement of $NaBH_4$ ligands used to stabilize Ag nanoparticles by **1** through a site-exchange reaction. Compound **1** contains a thiol function, which serves as an anchor to bind **1** to the surface of Ag(0) nanoparticles, and a thioxanthone moiety, which is suitable as an initiator group for photoinduced polymerization.

Received: October 2, 2012
Revised: November 13, 2012
Published: December 11, 2012

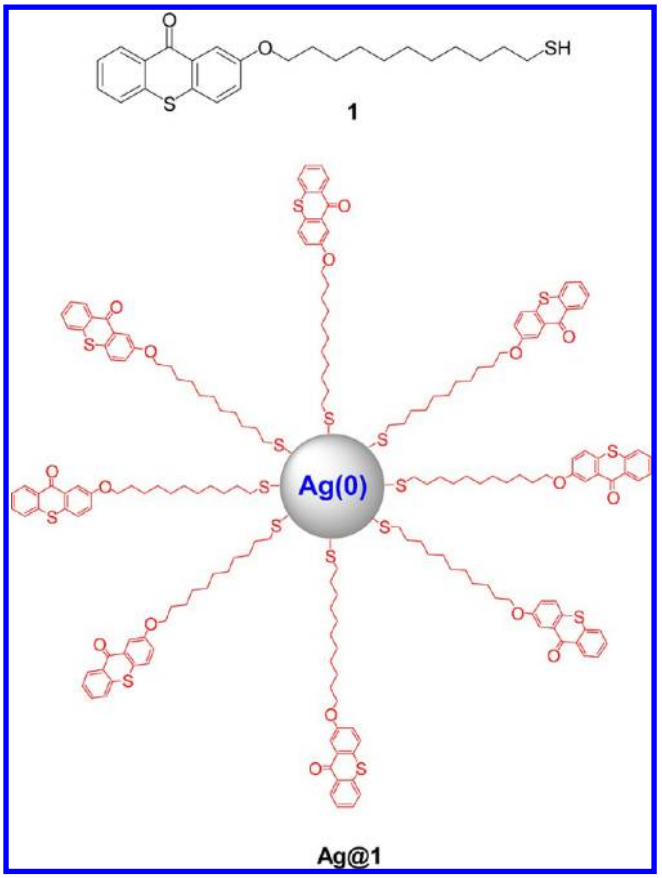

Figure 1. Structures of 2-(11-mercaptoundecyloxy)thioxanthone (**1**) and of Ag@**1** nanoparticles.

The site-exchange reaction leads therefore to Ag nanoparticles functionalized on their surface with radical initiator moieties. The Ag(0)@**1** nanoassembly was evaluated as a macro-photoinitiator for free radical polymerization of acrylate monomers. The functionalized Ag nanoparticles (Ag(0)@**1**) and Ag nanoparticles−polyacrylate nanocomposite were characterized by transmission electron microscopy, UV−vis and fluorescence spectroscopies, and X-ray photoelectron spectroscopy.

2. EXPERIMENTAL SECTION

2.1. Materials. Silver nitrate (≥99.8%), sodium borohydride (≥99%), thiosalicylic acid (97%), phenol (99%), 1,11-dibromoundecane (>98%), potassium thioacetate (98%), trifluoroacetic acid (99%), potassium carbonate (99.7%), and *N*-methyldiethanolamine (MDEA) were all purchased from Sigma-Aldrich and used as received. Ethoxylated(10) bisphenol dimethacrylate monomer (SR 480, M_w = 808 g/mol and viscosity at 25 °C = 410 cPs) was provided by Sartomer. All the solvents employed for synthesis and photophysical analyses were Sigma-Aldrich spectroscopic grade.

2.2. Synthesis of TX Derivatives. *2-(11′-Bromoundecyloxy)-9H-thioxanthen-9-one (**3**).* Under argon, 2-hydroxythioxanthone (**2**) (0.430 g, 1.89 mmol) and K_2CO_3 (0.300 g, 2.17 mmol) were dissolved in 12 mL of anhydrous DMF. After 5 min stirring at room temperature, 1,11-dibromoundecane (0.85 mL, 3.69 mmol) was added, and the mixture was refluxed for 6 h. After cooling, DMF was removed under reduced pressure, and the residue dissolved in dichloromethane (20 mL). The organic layer was then washed with water (5 mL), dried ($MgSO_4$), and concentrated in vacuo to yield an orange compound. Purification by column chromatography (SiO_2, petroleum ether−AcOEt 100:0 changing to petroleum ether−AcOEt 96:4) gave **3** as a yellow solid in 28% yield. ^{1}H NMR ($CDCl_3$, 300 MHz): δ 8.66 (d, J = 7.8 Hz, 1H), 8.10 (d, J = 2.8 Hz, 1H), 7.46 (m, 5H), 4.13 (t, J = 6.2 Hz, 2H), 3.44 (t, J = 6.9 Hz, 2H), 1.61 (m, 18 H). ^{13}C NMR ($CDCl_3$, 75 MHz): δ 179.7, 137.5, 132.0, 130.3, 129.9, 128.9, 128.7, 127.2, 126.0, 126.0, 123.0, 114.1, 111.2, 34.0, 33.8, 32.8, 29.5, 29.4, 29.3, 29.1, 28.9, 28.7, 28.2, 26.0.

*(2-Undecyloxy-9H-thioxanthen-9-one)ethanethioic Acid Ester (**4**).* Under argon, compound **3** (0.210 g, 0.456 mmol) was dissolved in acetone (8 mL). Potassium thioacetate (0.104 g, 0.911 mmol) was then added, and this mixture was stirred at room temperature for 18 h. Acetone was then removed under reduced pressure to yield a yellow residue. Purification by column chromatography (SiO_2, petroleum ether−AcOEt 99:1) gave **4** as a yellow solid in 83% yield. ^{1}H NMR ($CDCl_3$, 300 MHz): δ 8.58 (d, J = 7.7 Hz, 1H), 8.01 (d, J = 2.8 Hz, 1H), 7.36 (m, 5H), 4.04 (t, J = 6.6 Hz, 2H), 2.84 (t, J = 7.4 Hz, 2H), 2.29 (s, 3H), 1.54 (m, 18H). ^{13}C NMR ($CDCl_3$, 75 MHz): δ 196.5, 180.1, 138.0, 132.4, 130.7, 130.4, 129.3, 129.2, 127.7, 126.5, 123.5, 111.7, 69.0, 30.1, 29.9, 29.7, 23.4, 26.6.

*2-(11′-Thiooxyundecyl)-9H-thioxanthen-9-one (**1**).* Under argon, compound **4** (0.130 mg, 0.85 mmol) was dissolved in 1,4-dioxane (1.5 mL). Water (2.5 mL) was then added, and after 30 min stirring at room temperature trifluoroacetic acid (0.22 mL). This mixture was heated to reflux for 15 h. After cooling to room temperature, water (20 mL) was added and the mixture extracted with CH_2Cl_2 (3 × 20 mL). The combined organic layers were washed with water (60 mL), dried ($MgSO_4$), and concentrated in vacuo to yield **1** as a yellow solid. Purification by column chromatography (SiO_2, petroleum ether−AcOEt 99:1 changing for petroleum ether−AcOEt 98:2) gave **1** as a yellow solid in 79% yield. ^{1}H NMR ($CDCl_3$, 300 MHz): δ 8.67 (d, J = 7.8 Hz, 1H), 8.11 (d, J = 2.8 Hz, 1H), 7.48 (m, 5H), 4.14 (t, J = 6.6 Hz, 2H), 2.55 (td, 3J = 3J' = 7.4 Hz, 2H), 1.53 (m, 19H). ^{13}C NMR ($CDCl_3$, 75 MHz): δ 180.3, 138.2, 132.6, 130.9, 130.5, 129.5, 129.3, 127.9, 126.7, 126.6, 123.7, 111.8, 69.2, 37.7, 30.3, 30.1, 30.0, 29.8, 29.0, 26.7, 25.3.

2.3. Synthesis and Surface Functionalization of Silver Nanoparticles. Silver nanoparticles were prepared using a classical method.[21] An acetonitrile solution of $AgNO_3$ (10 mL of a 1.0 mM, 10^{-5} mol) was added dropwise under rapid stirring to a large excess of ice-cold sodium borohydride solution in acetonitrile (30 mL of a 2.0 mM solution, 6 × 10^{-5} mol). Sodium borohydride is used to both reduce Ag^+ and stabilize the silver nanoparticles resulting thereof. After addition of the whole of $AgNO_3$, the solution was further stirred for 27 min in the dark. The particles were isolated by centrifugation (4000 rpm for 15 min), washed with acetonitrile, and finally redispersed in 9 mL of acetonitrile under sonication.

3 mL of a 3.33 mM solution of 2-(11-mercaptoundecyloxy)-thioxanthone (**1**) in acetonitrile was added to the Ag NPs in acetonitrile, and the mixture was sonicated for 30 min. After the site-exchange reaction, Ag@**1** NPs were isolated by centrifugation (4000 rpm for 45 min.) and washed several times with acetonitrile in order to remove free **1**.

2.4. Photopolymerization. The **1**-capped silver nanoparticles (Ag@**1**) were dispersed into the polymerizable formulation (Figure 2)

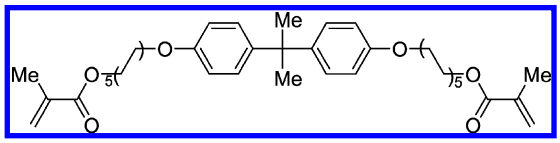

Figure 2. Chemical structure of the monomer ethoxylated (10) bisphenol dimethacrylate (SR 480).

and stirred for 1 h in the dark under a nitrogen atmosphere. The Ag@**1** NPs were introduced in the formulation at a concentration of 0.1 and 0.5 wt %. The photopolymerization was monitored by real-time Fourier transformed infrared spectroscopy (RT-FTIR). The laminated film was placed horizontally in the sample compartment of the spectrometer and exposed simultaneously to the IR probe beam and UV curing source (wavelength 377 nm). The conversion rates were

dx.doi.org/10.1021/la303923p | *Langmuir* 2012, 28, 17795−17802

Scheme 2. Synthesis Route toward Thioxanthone 1

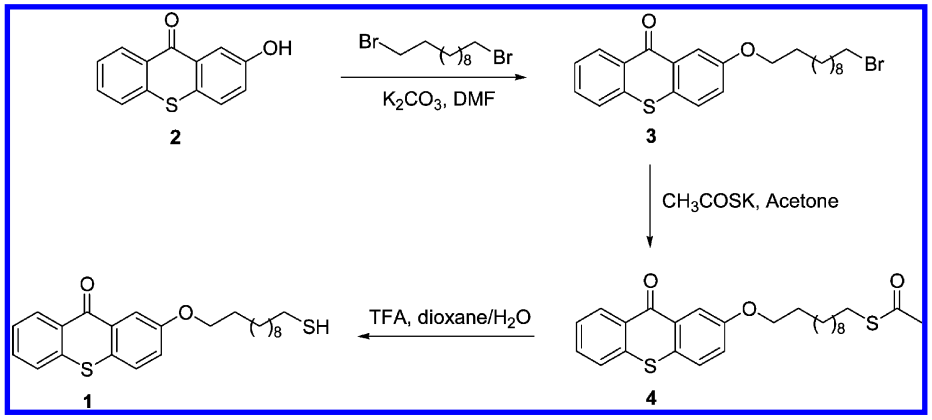

deduced from the disappearance of the characteristic bands of the acrylate double bond at 1635 cm^{-1}.

2.5. Instrumentation. The absorption measurements were carried out with a PerkinElmer Lambda 750 spectrometer, and a FluoroMax 4 HORIBA Jobin Yvon spectrofluorometer was used to record the fluorescence spectra. The emission spectra were spectrally corrected in all cases.

Transmission electron microscopy images (TEM) were obtained using a Philips CM20 instrument with LaB6 cathode operated at 200 kV. A drop of liquid formulations was placed onto a copper grid. As for the nanocomposites obtained after UV-cured, they were cut by means of a microtome (LKB model 8800) and placed onto the observation grid.

Powder X-ray diffraction (XRD) was performed using a Philips X'Pert diffractometer equipped with a general area detector diffraction system with Cu Kα radiation. Samples were placed on a 1 mm thick silicon substrate under operating conditions of 40 kV and 40 mA.

X-ray photoelectron spectroscopy (XPS) measurements were performed on a KRATOS Axis Ultra electron energy analyzer operating with an Al Kα monochromatic source.

The photopolymerization was monitored with a Nicolet 8700 RT-FTIR spectrometer, from Thermo Fisher Scientific. The laminated formulation (20 μm thick), deposited on a BaF_2 pellet, was irradiated at 377 nm with a laser diode from Coherent.

3. RESULTS AND DISCUSSION

3.1. Synthesis and Optical Properties of 1. The synthesis route toward thioxanthone **1** is depicted in Scheme 2. The starting 2-hydroxythioxanthone (**2**) was prepared from a literature procedure,[22] which involved heating of thiosalicylic acid and phenol in the presence of sulfuric acid. Compound **2** was alkylated using 1,11-dibromoundecane and K_2CO_3 in refluxing DMF to afford **3** in 28% yield,[23] accompanied by 37% of a bis(thioxanthone) arising from disubstitution on 1,11-dibromoundecane. Subsequent treatment of **3** with potassium thioacetate in acetone followed by acid hydrolysis[24] of thioester **4** furnished the targeted 2-(11-mercaptoundecyloxy)-thioxanthone (**1**).

3.2. Photophysical Properties of Compound 1. The photophysical properties of 2-(11-mercaptoundecyloxy)-thioxanthone (**1**) are shown in Figure 3 and Table 1 along with those of 2-methoxythioxanthone used as reference. Compound **1** exhibits an absorption band located in the 350−400 nm range which corresponds to the superimposition of two electronic transitions which are energetically very close: a forbidden S0−S2 transition (n−π*) which is mainly localized on the carbonyl function and a strongly allowed S0−S1 transition (π−π*) which involves an electronic delocalization in the aromatic ring. The spectroscopic properties of compound **1**

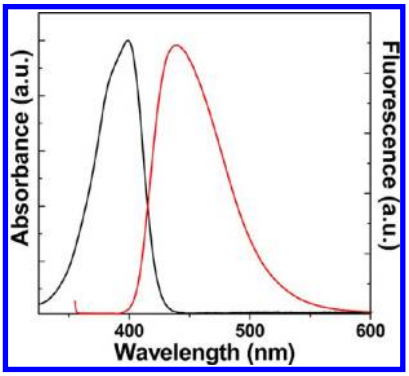

Figure 3. Normalized absorption (black line) and fluorescence (red line) spectra of 2-(11-mercaptoundecyloxy)thioxanthone in acetonitrile.

Table 1. Spectroscopic Data of 2-Methoxythioxanthone and 2-(11-Mercaptoundecyloxy)thioxanthone (1) in Ethyl Acetate and Acetonitrile, Respectively

	λ_{abs} (nm)	λ_{em} (nm) (λ_{ex} = 350 nm)	ε_{abs} (M^{-1} cm^{-1})	Φ_{fluo}
2-MeOTX[25]	395	425	2400	0.025
1	386	440	6100	0.115

were very similar to those of reference 2-MeOTX derivative. The absorption band of **1** is centered at 386 nm with an absorption coefficient of 6100 M^{-1} cm^{-1}, and the emission spectrum is centered at 440 nm (Figure 3).

3.3. Synthesis of Ag@1 Nanoparticles. An intense characteristic surface plasmon band located at 403 nm can be observed in the UV−vis absorption spectrum immediately after synthesis of Ag(0) NPs using $NaBH_4$ as reductant of $AgNO_3$ (Figure 4). Silver nanoparticles were next functionalized with 2-(11-mercaptoundecyloxy)thioxanthone (**1**), so that nanoparticles and xanthenic heterocycles are separated by a 12-atom spacer. At room temperature, Ag(0) NPs were dispersed in a solution of thioxanthone **1** in acetonitrile. The UV−vis spectra show an absorption band centered at 383 nm corresponding to the thioxanthone moiety and the plasmon band of the Ag NPs. The grafting of TX chromophores onto silver nanoparticles was monitored by recording absorption spectra every 5 min for 30 min. As illustrated in Figure 4, the anchorage of compound **1** at the periphery of Ag NPs occurs immediately after mixing and extended exposure does not change the optical properties of the nanohybrids. After several

dx.doi.org/10.1021/la303923p | Langmuir 2012, 28, 17795−17802

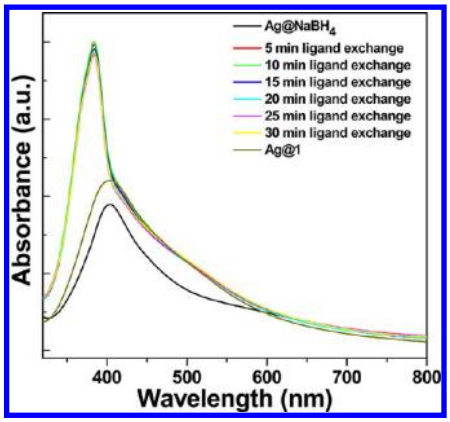

Figure 4. Evolution of the absorption spectra of silver nanoparticles during ligand exchange with thioxanthone **1**.

washing with acetonitrile to remove the excess of **1** that did not anchor on nanoparticles, Ag@**1** NPs were characterized by UV−vis spectra. The maximum of the surface plasmon band is at 404 nm, but a broadening was observed compared to the native $NaBH_4$-capped Ag NPs. This change suggests that aggregation may have occurred during cap ligand exchange (Figure 4). We also noted that thioxanthone **1** adsorbs very efficiently on Ag NPs. Using the molar extinction coefficient ε = 6100 M^{-1} cm^{-1} at 399 nm of **1**, we estimated than only ca. 4% of **1** remained in solution after the ligand exchange step and that ca. 96% of **1** introduced in the reaction mixture was linked to Ag NPs. Finally, when stored at room temperature and in the dark, the functionalized Ag@**1** NPs exhibit excellent stability (over several months).

3.4. Characterization of the Ag@1 Nanoparticles. The functionalized Ag@**1** NPs were characterized by X-ray diffraction, transmission electron microscopy, and X-ray photoelectron spectroscopy.

The X-ray diffraction analysis confirms the presence of silver nanoparticles with a high degree of crystallinity. Figure 5 shows

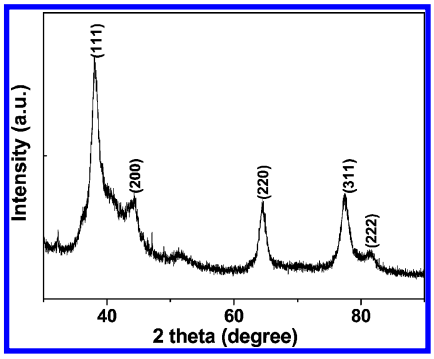

Figure 5. XRD patterns of as-synthesized Ag@**1** nanoparticles.

the XRD patterns of the sample; the presence of peaks corresponding to diffraction by (111), (200), (220), (311), and (222) planes indicates a face-centered cubic (fcc) crystalline structure of the silver nanoparticles (JCPDS 04-0783). According to the Laue−Scherrer equation, the average size of the silver crystalline domains is equal to 5.7 ± 1 nm. Very weak reflections of residual $AgNO_3$ can also be observed on the diffractogram at 2θ = 33° and 36°.

Using transmission electron microscopy (TEM), Ag@**1** nanoparticles appear spherical in shape (Figure 6a). A statistic analysis on a population of 100 particles provides a size distribution histogram with an average diameter of ca. 5−6 nm (Figure 6b). The TEM analysis shows a good agreement with XRD measurements.

X-ray photoelectron spectroscopy (XPS) analysis was performed to investigate the surface chemistry of Ag@**1** NPs. The survey spectrum of Ag@**1** NPs identified the presence of Ag, C, O, and S (Figure 7a). The high-resolution spectrum of Ag 3d is given in Figure 7b. The spectrum shows the Ag 3d splitting into Ag $3d_{3/2}$ (373.6 eV) and Ag $3d_{5/2}$ (367.4 eV) peaks with a peak separation of 6.2 eV and confirms that the valence state of silver element is Ag(0).

3.5. Photophysical Properties of the Ag(0)@1 Nanoassembly. Regarding the luminescence of the Ag@**1** nanoassemblies, no fluorescence signal was detected over the range 300−700 nm, thus strongly suggesting a complete quenching of the radiative deactivation of **1** grafted onto the Ag(0) NPs. Such a behavior was already reported by several authors; it was rationalized as the result of competition between quenching rate enforced by energy-transfer process and the increased excitation rate induced by local electromagnetic field on the metal surface.[26−28]

The technique introduced by Romani[29] was used to evaluate intersystem crossing quantum yield Φ_{ISC} of the free **1** and grafted Ag@**1** NPs. It consists in quenching the triplet state of **1** by camphorquinone (CQ) and measuring the corresponding phosphorescence of CQ at room temperature. The triplet quantum yield is then deduced by comparing the intensity of this emission with what is obtained when compound **1** is replaced by a reference donor whose Φ_{ISC} is known. Unfortunately, the determination of the intersystem crossing quantum yields (Φ_{ISC}) of free **1** was impossible because of the intramolecular hydrogen abstraction that takes place between the carbonyl in its triplet state and the thiol group. Because of the fact that the spacer is likely to fold and allow the −SH group to come close to the carbonyl, this hydrogen abstraction proceeds much faster that the bimolecular reaction of triplet **1** with CQ, whatever the concentration of the quencher. Such an intramolecular interaction was already reported by Turro et al. in the case of a thioxanthone.[30] To confirm this hypothesis, the S-ethylated derivative of **1** was prepared. The abstractable hydrogen is no longer available in this compound, and the phosphorescence of CQ was readily observed and Φ_{ISC} was determined to be 0.35 in acetonitrile. At the same time when the **1** moiety was grafted onto metal particles, the Φ_{ISC} was determined to be 0.65 in acetonitrile, of the same order as the triplet quantum yield of free TX under the same experimental conditions.

3.6. Photopolymerization. Scheme 3 shows the proposed mechanism for the photopolymerization of an acrylic monomer initiated by Ag@**1** NPs.

The following formulation used to fabricate polymer/silver nanocomposite contained a difunctional methacrylate monomer, ethoxylated (10) bisphenol dimethacrylate (SR 480), 0.1 or 0.5 wt % Ag(0)@**1** NPs and 4% MDEA. The irradiation was carried out at 377 nm (10 mW cm^{-2}). Figure 8 compares the conversion rates achieved with 0.5 wt % Ag(0)@**1**, 0.1 wt % Ag(0)@**1**, and the reference compound **1** (0.5 wt %). The degree of conversion of the samples exposed to UV light was evaluated after a 120 s exposure. Samples containing compound **1** and Ag@**1** NPs at a concentration of 0.5 wt % showed a similar ultimate degree of conversion (within experimental error, ca. 98% and 95%, respectively). However, an important

dx.doi.org/10.1021/la303923p | *Langmuir* 2012, 28, 17795−17802

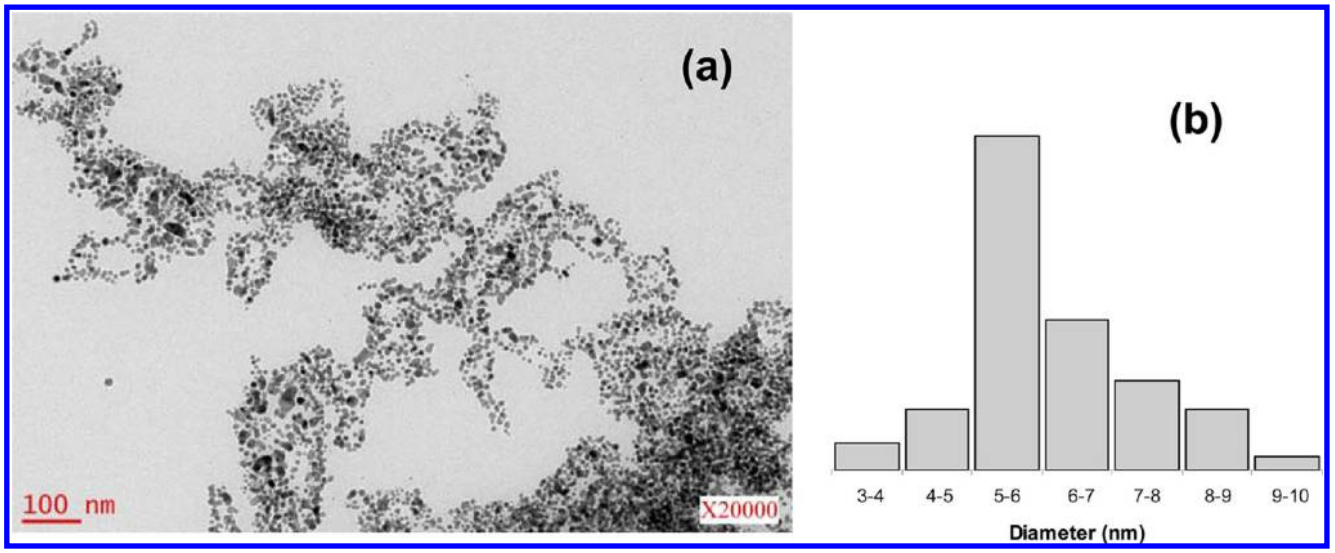

Figure 6. (a) Bright-field TEM micrograph of Ag@**1** nanoparticles and (b) the corresponding size distribution.

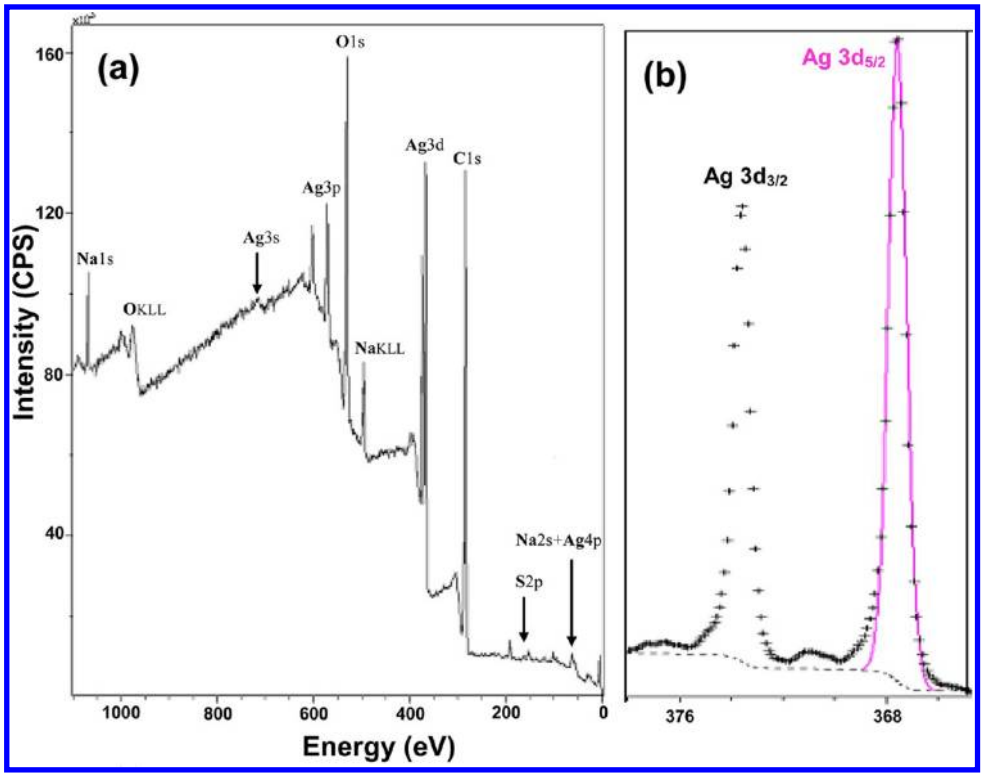

Figure 7. (a) XPS survey spectrum of Ag@**1** NPs and (b) high-resolution spectrum of Ag 3d.

difference on the rate of polymerization (R_p) was visible (R_p is defined as the value of the first derivative of the conversion vs time curves). Thus, R_p at time zero was measured to be 2.0 and 2.6 M L^{-1} s^{-1} with and without metal nanoparticles (0.5 wt %), respectively. At maximum, the rates of conversion are in the ratio of 2.0 to 3.5 M L^{-1} s^{-1}. The presence of Ag NPs can induce a decrease of the rate of polymerization, but the degree of conversion after 120 s exposures is similar. In the presence of a smaller amount of Ag@**1** NPs (0.1 wt %), the final degree of conversion decreased to ca. 76% and R_p to 1.6 M L^{-1} s^{-1}. This effect was mainly due to a weakest absorption of the actinic photons.

Figure 9a shows a TEM image of the photocured film with 0.5 wt % Ag@**1** as photoinitiator. The nanoparticles appear very well dispersed and without aggregation. A statistic analysis on a population of 300 particles provides a size distribution histogram with an average diameter of 5.6 nm (Figure 6b).

The polymer films with and without NPs were analyzed using SEM (Figure 10). These films confirm the potential in photoinduced processes of the Ag NPs grafted chromophores as new photoinitiators to develop silver/polymer nanocomposites through a photopolymerization process. Chemically linking Ag NPs to a polymer matrix offers the advantages over composite materials obtained from mechanically dispersed formulations of a much better dispersibility without aggregation

dx.doi.org/10.1021/la303923p | *Langmuir* 2012, 28, 17795−17802

Scheme 3. Schematic Mechanism for the Photopolymerization Initiated by the Ag@1 Nanoparticles

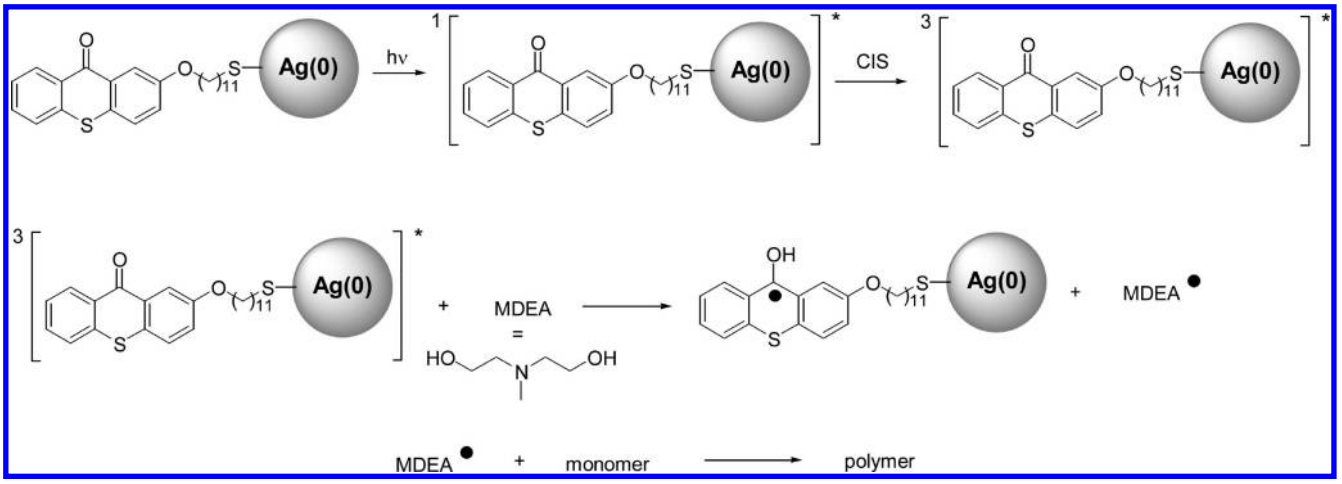

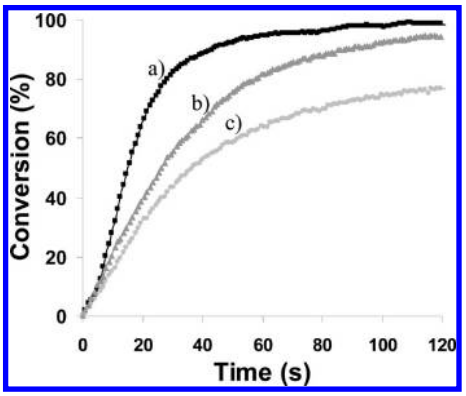

Figure 8. Real-time kinetic conversion curves for UV curing at 377 nm (a) 0.5 wt % compound **1**, (b) 0.5 wt % Ag@**1** NPs, and (c) 0.1 wt % Ag@**1** NPs. Light intensity = 10 mW cm^{-2}; thickness = 12 μm.

that strongly influences the final properties of the composite material.[31,32] Figure 10 shows a clear difference in the morphology of the surface of nanocomposites films. These are homogeneous, with more or less periodical wrinkles. In the case where a very small amount of Ag@**1** NPs (0.1 wt %) was present, the surface of the film was wrinkled with a more or less marked corrugation at the 10 nm scale which is oriented aleatorily, whereas with 0.5 wt % Ag@**1**, it was irregular but with a less pronounced relief of which some prominences are emerging. These morphological differences of the polymers composite films could be related to the chemical nature of the initiating systems; the presence of nanoparticles can generate this wrinkling or buckling phenomena.[33,34]

4. CONCLUSIONS

Ag NPs were synthesized and functionalized by 2-(11-mercaptoundecyloxy)thioxanthone (**1**). The influence of the plasmon field generated in the immediate vicinity of the metal particle and **1** was studied. Ag@**1** NPs were used as a new class of type II photoinitiator in radical photopolymerization reactions to obtain organic/inorganic nanocomposites. It was exemplified by the radical photopolymerization of a bis-(methacrylate) monomer. This new class of photoinitiating structure was found to offer new interesting vistas for patterning thin film or for engraving information at their

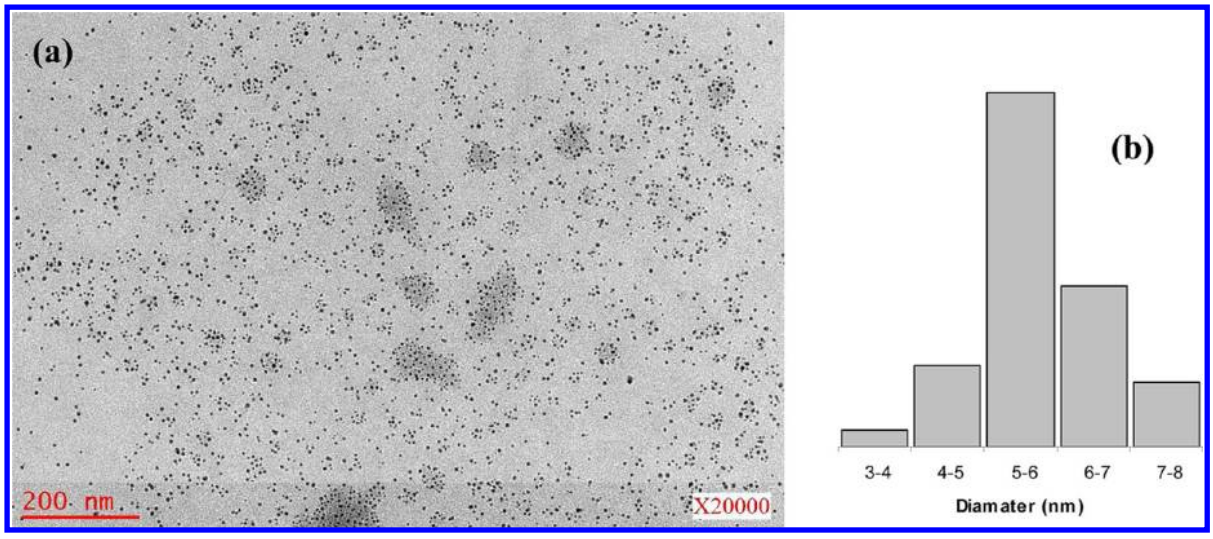

Figure 9. (a) Bright-field TEM micrograph of silver nanoparticles in the polymer matrix containing ethoxylated (10) bisphenol dimethacrylate (SR 480), 0.5 wt % Ag(0)@**1** NPs and 4% MDEA. (b) The corresponding size distribution. The irradiation was carried out at 377 nm (10 mW cm^{-2}) and 12 μm thickness.

dx.doi.org/10.1021/la303923p | *Langmuir* 2012, 28, 17795−17802

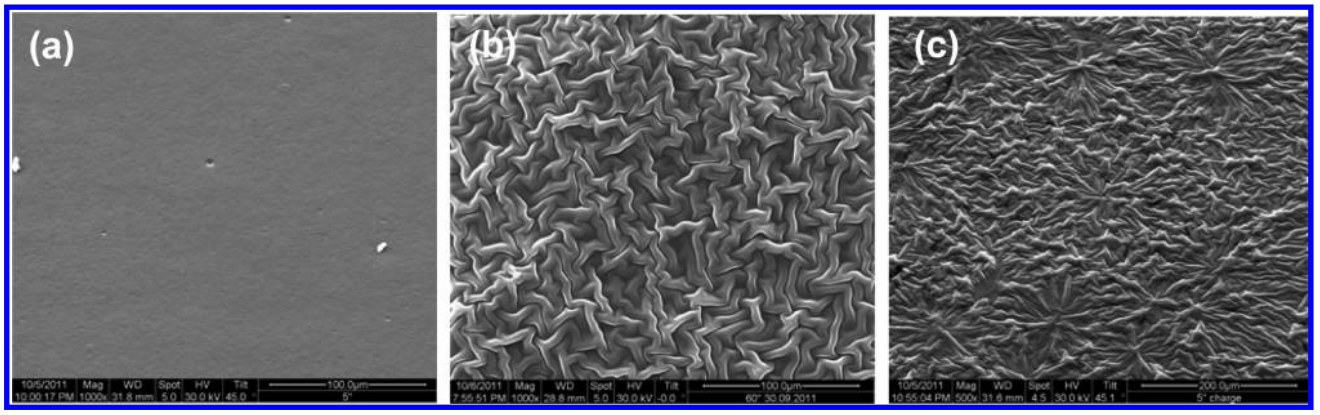

Figure 10. SEM images of (a) polymer without Ag@**1** NPs and (b) and (c) silver/polymer nanocomposites prepared with 0.1 wt %Ag@**1** and 0.5 wt % Ag@**1**, respectively.

surface. Its innovative character lies in the fact that it induces the formation of a diffusive surface. Additional studies on particle size and shape effects on the photopolymerization are under way.

This Ag(0)@**1** nanoassembly can also lend itself to the fabrication of metal/polymer nanoobjects.

AUTHOR INFORMATION

Corresponding Author

*E-mail lavinia.balan@uha.fr.

Notes

The authors declare no competing financial interest.

ACKNOWLEDGMENTS

The authors thank the Agence Nationale de la Recherche (ANR) for financial support under Contract ANR-09-JCJC-0029-01.

REFERENCES

(1) Kelly, K. L.; Coronado, E.; Zhao, L. L.; Schatze, G. C. The Optical Properties of Metal Nanoparticles: The Influence of Size, Shape, and Dielectric Environment. *J. Phys. Chem. B* **2003**, *107*, 668−677.

(2) Karim, M. R.; Lim, K. T.; Lee, C. J.; Bhuiyan, M. T. I.; Kin, H. J.; Park, L. S.; Lee, M. S. Synthesis of Core-Shell Silver−Polyaniline Nanocomposites by Gamma Radiolysis Method. *J. Polym. Sci., Part A: Polym. Chem.* **2007**, *45*, 5741−5747.

(3) Balan, L.; Turck, C.; Soppera, O.; Lougnot, D. J. Holographic Recording with Polymer Nanocomposites Containing Silver Nanoparticles Photogenerated in Situ by the Interference Pattern. *Chem. Mater.* **2009**, *21*, 5711−5718.

(4) Porel, S.; Singh, S.; Harsha, S. S.; Rao, D. N.; Radhakrishnan, T. P. Nanoparticle-Embedded Polymer: In situ Synthesis, Free-Standing Films with Highly Monodisperse Silver Nanoparticles and Optical Limiting. *Chem. Mater.* **2005**, *17*, 9−12.

(5) Korchev, A. S.; Bozack, M. J.; Slaten, B. L.; Mills, G. Polymer-Initiated Photogeneration of Silver Nanoparticles in SPEEK/PVA films: Direct Metal Photopatterning. *J. Am. Chem. Soc.* **2004**, *126*, 10−11.

(6) Sangermano, M.; Yagci, Y.; Rizza, G. In situ Synthesis of Silver-Epoxy Nanocomposites by Photoinduced Electron Transfer and Cationic Polymerization Processes. *Macromolecules* **2007**, *40*, 8827−8829.

(7) Sudeep, P. K.; Kamat, P. V. Photosensitized Growth of Silver Nanoparticles under Visible Light Irradiation: A Mechanistic Investigation. *Chem. Mater.* **2005**, *17*, 5404−5410.

(8) Balan, L.; Jin, M.; Malval, J. P.; Chaumeil, H.; Defoin, A.; Vidal, L. Fabrication of Silver Nanoparticle-Embedded Polymer Promoted by Combined Photochemical Properties of a 2,7-Diaminofluorene Derivative Dye. *Macromolecules* **2008**, *41*, 9359−9365.

(9) Balan, L.; Malval, J. P.; Le Nouen, D.; Schneider, R.; Lougnot, D. J. In-situ Fabrication of Polyacrylate-Silver Nanocomposite through Photoinduced Tandem Reactions Involving Eosin Dye. *Polymer* **2010**, *51*, 1363−1369.

(10) Cook, W. D.; Nghiem, Q. D.; Chen, Q.; Chen, F.; Sangermano, M. Simultaneous Photoinduced Silver Nanoparticles Formation and Cationic Polymerization of Divinyl Ethers. *Macromolecules* **2011**, *44*, 4065−4071.

(11) Malval, J. P.; Jin, M.; Balan, L.; Schneider, R.; Versace, D. L.; Chaumeil, H.; Defoin, A.; Soppera, O. Photoinduced Size-Controlled Generation of Silver Nanoparticles Coated with Carboxylate-Derivatized Thioxanthones. *J. Phys. Chem. C* **2010**, *114*, 10396−10402.

(12) Selvan, S. T.; Spatz, J. P.; Klok, H.-A.; Möller, M. Gold-Polypyrrole Core-shell Particles in Diblock Copolymer Micelles. *Adv. Mater.* **1998**, *10*, 132.

(13) Nuss, S.; Böttcher, H.; Wurm, H.; Hallensleben, M. L. Gold Nanoparticles with Covalently Attached Polymer Chains. *Angew. Chem., Int. Ed.* **2001**, *40*, 4016.

(14) Mandal, T. K.; Fleming, M. S.; Walt, D. R. Preparation of Polymer Coated Gold Nanoparticles by Surface-Confined Living Radical Polymerization at Ambient Temperature. *Nano Lett.* **2002**, *2*, 3−7.

(15) Brust, M.; Walker, M.; Bethell, D.; Schiffrin, D. J.; Whyman, R. Synthesis of Thiol-derivatised Gold Nanoparticles in Two-phase Liquid-Liquid System. *J. Chem. Soc., Chem. Commun.* **1994**, 801−802.

(16) Goulet, P. J. G.; Lennox, B. R. New Insights into Brust-Schiffrin Metal Nanoparticle Synthesis. *J. Am. Chem. Soc.* **2010**, *132*, 9582−9584.

(17) Yagci, Y.; Onen, A. Bifunctional Initiators 0.3. Photochemical-Synthsis of Block Copolymers of Styrene and Methyl-Methacrylate with the aid of Azo-Benzoin Initiators. *J. Macromol. Sci., Part A: Chem.* **1991**, *A28*, 129−141.

(18) Onen, A.; Yagci, Y. Bifunctional Initiators; Synthesis, Characterization, and Initiator Properties of Azo-benzoin Initiators. *J. Macromol. Sci., Part A: Chem.* **1990**, *A27*, 743−753.

(19) Fouassier, J. P. *Photoinitiating Systems in Radiation Curing in Polymer Science and Technology: Photoinitiating Systems*; Elsevier Applied Science: Amsterdam, 1993.

(20) Karasu, F.; Arsu, N.; Yagci, Y. 2-Mercapto Thioxanthone as a Chain Transfer Agent in Free-Radical Polymerization: A Versatile Route to Incorporate Thioxanthone Moieties into Polymer Chain-ends. *J. Appl. Polym. Sci.* **2007**, *103*, 3766−3770.

(21) Solomon, S. D.; Bahadory, M.; Jeyarajasingam, A. V.; Rutkowsky, S. A.; Boritz, C. Synthesis and Study of Silver Nanoparticles. *J. Chem. Educ.* **2007**, *84*, 322−325.

(22) Aydin, M.; Arsu, N.; Yagci, Y. One-component Bimolecular Photoinitiating Systems, 2 - Thioxanthone acetic acid Derivatives as

Photoinitiators for Free Radical Polymerization. *Macromol. Rapid Commun.* **2003**, *24*, 718−723.
(23) Sivakova, S.; Wu, J.; Campo, C. J.; Mather, P. T.; Rowan, S. J. Liquid-Crystalline Supramolecular Polymers Formed through Complementary Nucleobase-pair Interactions. *Chem.—Eur. J.* **2005**, *12*, 446−456.
(24) Iimura, S.; Manabe, K.; Kobayashi, S. Hydrophobic Polymer-Supported Catalyst for Organic Reactions in Water: Acid-Catalyzed Hydrolysis of Thioesters and Transprotection of Thiols. *Org. Lett.* **2003**, *5*, 101−103.
(25) Merkel, P. B.; Dinnocenzo, J. P. Thermodynamic Energies of Donor and Acceptor Triplet States. *Photochem. Photobiol. A: Chem.* **2008**, *193*, 110−121.
(26) Evanoff, D. D.; White, R. L.; Chumanov, G. Measuring the Distance Dependence of the Local Electromagnetic Field from Silver Nanoparticles. *J. Phys. Chem. B* **2004**, *108*, 1522−1524.
(27) Anger, P.; Bharadwaj, P.; Novotny, L. Enhancement and Quenching of Single-Molecule Fluorescence. *Phys. Rev. Lett.* **2006**, *96*, 113002.
(28) Stamplecoskie, K. G.; Scaiano, J. C. Silver as an Example of the Applications of Photochemistry to the Synthesis and Uses of Nanomaterials. *Photochem. Photobiol.* **2012**, *88*, 762−768.
(29) Romani, A.; Favaro, G.; Masetti, F. Luminescence Properties of Camphorquinone at Room Temperature. *J. Lumin.* **1995**, *63*, 183−188.
(30) Aydin, M.; Arsu, N.; Yagci, Y.; Jockusch, S.; Turro, N. J. Mechanistic Study of Photoinitiated Free Radical Polymerization Using Thioxanthone Thioacetic Acid as One-Component Type II Photoinitiator. *Macromolecules* **2005**, *38*, 4133−4138.
(31) Kong, H.; Jang, J. Antibacterial Properties of Novel Poly(methyl methacrylate) Nanofiber Containing Silver Nanoparticles. *Langmuir* **2008**, *24*, 2051−2056.
(32) Buruiana, T.; Melinte, V.; Chibac, A.; Matiut, S.; Balan, L. Synthesis, Evaluation and Preliminary Antibacterial Testing of Hybrid Composites Based on Urethane Oligodimethacrylates and Ag Nanoparticles. *J. Biomater. Sci., Polym. Ed.* **2012**, *23*, 955−972.
(33) Basu, S. K.; Scriven, L. E.; Francis, L. F.; McCormick, A. V. Mechanism of Wrinkle Formation in Curing Coatings. *Prog. Org. Coat.* **2005**, *53* (1), 1−16.
(34) Samyn, P.; Laborie, M.-P.; Mathew, A. P.; Airoudj, A.; Haidara, H.; Roucoules, V. Metastable Patterning of Plasma Nanocomposite Films by Incorporating Cellulose Nanowhiskers. *Langmuir* **2012**, *28*, 1427−1438.